Archives of Microbiology (2025) 207:4
https://doi.org/10.1007/s00203-024-04207-w

ORIGINAL PAPER

Biopolymer-based oral films integrated with probiotic active compounds for improved health applications

Sinem Tunçer Çağlayan[1]

Received: 18 September 2024 / Accepted: 18 November 2024 / Published online: 28 November 2024

Abstract

Orally dissolving films (ODFs) have emerged as a versatile platform that combines convenience, efficacy, and patient compliance. In this study, the cell-free supernatant of the oral probiotic *Streptococcus salivarius* M18 was incorporated into various biopolymer-based ODF formulations, evaluated for demolding, fragility, and flexibility. The combination of carboxymethyl cellulose, sodium alginate, and glycerol successfully formed stable films. The films were characterized by weight, thickness, pH, and disintegration times. Fourier-transform infrared spectroscopy (FTIR) was used to analyze ODF content and release profiles in simulated saliva. Unique absorption peaks in the cell-free product-incorporated ODF samples confirmed the integration of bacterial proteins, lipids, and nucleic acids into the ODF matrix. The biological activity of the ODF carrying M18 bioactive products was assessed by its inhibitory effect on the growth of *Streptococcus mutans*, a pathogen linked to dental plaque and cavities. Additionally, the anti-proliferative effect on cancer epithelial cells was demonstrated. This study show that probiotic products can be integrated into bio-based thin films without losing activity, making this delivery platform promising for local and potentially systemic effects.

Keywords Orally dissolving film (ODF) · Carboxymethyl cellulose · Alginate · Probiotics · *Streptococcus salivarius* M18 · *Streptococcus mutans*

Introduction

The oral microbiota plays a crucial role in maintaining the homeostasis of the oral environment, with microorganisms deriving nourishment from saliva and gingival crevicular fluid. However, alterations in the structure of the oral microbiome can lead to the development of caries, enamel erosion, and periodontal disease. According to the World Health Organization (WHO), approximately half of the global population suffers from oral diseases, with 2.4 billion people experiencing permanent tooth decay and 532 million children affected by primary tooth decay. Once an infection occurs, the available treatment options are not only painful but also come with a high cost and time commitment (Chugh et al. 2020; Jung et al. 2021; Homayouni Rad et al. 2023).

Tooth decay arises from a combination of factors, including a cariogenic diet, poor oral hygiene, high levels of cariogenic bacteria, dental plaque, reduced saliva flow, and inadequate exposure to fluoride (Javed et al. 2023). Numerous studies underscore the close relationship between the composition of oral microbiota and oral health, highlighting the critical role of microbiota disruption in oral diseases (Morrison et al. 2023). Both in vitro and in vivo studies have explored the potential of probiotics in preventing or treating periodontal diseases and tooth decay as a promising alternative to antibiotics (Abikshyeet et al. 2022). The mechanisms underlying the action of probiotics on oral health align with those observed in gastrointestinal studies. Evidence suggests that probiotics exert antimicrobial effects through the production of substances such as bacteriocins, organic acids, fatty acids, and hydrogen peroxide (Homayouni Rad et al. 2023). However, despite numerous studies suggesting the potential benefits of probiotic usage, there is a lack of clear regulations regarding clinical recommendations for probiotic consumption. This includes aspects such

Communicated by Christopher Franco.

✉ Sinem Tunçer Çağlayan
sinem.tuncer@bilecik.edu.tr

[1] Vocational School of Health Services, Department of Medical Services and Techniques, Bilecik Şeyh Edebali University, Bilecik 11100, Turkey

as the selection of appropriate probiotics, control of their dietary intake, and timing and frequency of probiotic dosing. Furthermore, the theoretical association of probiotic consumption with undesirable side effects, such as systemic infections, deleterious metabolic activities, and excessive immune stimulation, has been proposed. Additional risks include unpredictable niche-specific actions and metabolite production, host-induced gene expressions, antibiotic resistance, the potential for opportunistic infections, interference with the colonization of commensal gut microflora, and bacterial translocation to tissue or blood. Moreover, there are technological concerns related to probiotic production, such as decreased viability, which limits the full potential applications of live cell probiotics in the food and pharmaceutical sectors. Risks of microbiological and non-microbial contamination, including allergens, various toxins, and heavy metals, also pose challenges. To address some of the obstacles associated with live probiotics, researchers are exploring the use of non-viable bacteria, bacterial compounds, or probiotic metabolites that exhibit similar or even enhanced health-improving biological activities compared to live probiotics. While health strategies centered around nutrition emphasize the utilization of commensal bacteria as probiotics, increasing evidence indicates that the health benefits ascribed to certain live probiotics are associated with the biomolecules derived from these microorganisms (Karaçam and Tunçer 2022; Homayouni Rad et al. 2023).

The bacterial replacement probiotic, *Streptococcus salivarius* strain M18, is derived specifically from the oral cavity and formulated for oral use. In 2019, the US Food and Drug Administration (FDA) designated *S. salivarius* M18 as Generally Recognized as Safe (GRAS; Notice No. 807) for incorporation into food, affirming that the strain can be used without causing harm to consumers (Karaçam and Tunçer 2023). Research on the inhibitory effects of *S. salivarius* M18 has primarily focused on bacterial species potentially associated with dental caries development. *Streptococcus mutans*, a bacterium in the oral microflora, stands out as a primary cause of dental decay (Heng 2016). Several clinical studies across diverse populations have highlighted the correlation between *S. mutans* levels and the incidence of caries (Spatafora et al. 2024). Previous reports have demonstrated the inhibitory effects of the probiotic *S. salivarius* M18 on various nasal, oral, and throat pathogens, including *S. mutans* (Tunçer and Karaçam 2020; Reichardt et al. 2024). Here, it is demonstrated that the cell-free supernatant of *S. salivarius* M18 is also capable of suppressing the growth of *S. mutans*. Leveraging this effect, the lyophilized supernatant was incorporated into orally dissolving films (ODFs), providing advantages over traditional oral dosages such as enhanced bioavailability and improved patient compliance, especially for children and individuals with swallowing difficulties (He et al. 2021).

This manuscript includes optimization processes for the mechanical suitability of the films to be incorporated with the bacterial products as well as sterilization to ensure their use for biological activity investigation studies. The produced films were characterized in terms of weight, thickness, pH, and disintegration times. The films and their release profiles were analyzed and discussed in detail using Fourier-transform infrared spectroscopy (FTIR). The biological activity of the film was investigated in saliva by examining its pathogen-inhibitory effect. Finally, considering recent findings indicating oral-colon interaction (Koliarakis et al. 2019; Kudra et al. 2023) and previously obtained results regarding the anti-tumor activity of *S. salivarius* M18 cell-free supernatant in colorectal cancer, the antiproliferative effect of the oral film was demonstrated in vitro on the colorectal cancer cell line (Karaçam and Tunçer 2022).

Materials and methods

Probiotic growth, cell-free supernatant preparation and lyophilization

S. salivarius M18 (BLIS Technologies, New Zealand) was cultured at 37ºC in Tryptic Soy Broth (TSB; pH 7.1–7.5) medium (cat. no: 1.05459; Merck Millipore, Burlington, MA, USA) either in a shaker incubator or on agar plates (1.5% w/v agar in TSB). The cell-free supernatants of the probiotic were obtained as described previously (Karaçam and Tunçer 2022, 2023). Briefly, the OD_{600} of overnight cultures was adjusted to 0.1, and the bacteria were grown for 24 h at 37ºC using a shaking incubator at 160 rpm in screw cap tubes filled with the growth medium. The tubes were sealed with paraffin film to create low oxygen (microaerobic) conditions. After 24 h, the cultures were centrifuged at 5000 rpm (1844xg) for 10 min at + 4ºC to collect the supernatants. The supernatants were then filtered through 0.22 µm PES (Polyethersulfone) membrane filters and stored at -80ºC before use. Lyophilization of the samples was carried out as described previously by a freeze dryer/lyophilizer (Biobase, China) (Tunçer and Karaçam 2020). The lyophilized samples were rehydrated in sterile dH_2O to prepare 1000 mg/ml. As a control, the lyophilized and rehydrated growth medium (TSB) was used (only medium = OM).

In the oral cavity, saliva's buffering capacity typically maintains a near-neutral pH (6.7–7.3) (Baliga et al. 2013); however, this buffering effect decreases when the pH drops to around 5.5, a threshold critical for dental enamel protection (Zhang et al. 2022). M18 growth reduces the pH of the environment around pH 5.0. Therefore, the pH of the

cell-free supernatant or lyophilized and rehydrated culture supernatant was adjusted to 7.0 (matching the pH of the lyophilized growth medium, OM) using 1.0 N sterile NaOH (2.0% v/v) to mimic the healthy oral cavity conditions and demonstrate that organic acids produced by the probiotic are not the sole effector molecules responsible for pathogen inhibition. An equal volume of sterile dH_2O was added to the OM control (Tunçer and Karaçam 2020).

Preparation of orally dissolving film formulations and characterization of the films

For film formation, Hydroxypropyl Methylcellulose (HPMC; Cat no: 423173-100G, Sigma, St. Louis, Missouri, USA), Guar Gum (GG; Cat no: G4129-250G, Sigma), Carboxymethyl Cellulose (CMC; food-grade CMC-E466, Alfasol, Turkey), and Sodium Alginate (SA; E401, food-grade, Alfasol, Turkey) were used as biopolymers, while sorbitol (%70, Cat no: ZK.101081, ZAG-SORBİTOL, ZAG Kimya, Turkey) and glycerol (87%, Cat no: 49782, Fluka) were employed as plasticizing agents. The polymerizing agents and plasticizers were used in various ratios and combinations for optimization studies, as presented in the results section.

The films were prepared as described by Ouda et al. (Ouda et al. 2020) with some modifications. In summary, the polymers were added to sterilized dH_2O pre-heated to 40 °C and mixed using a magnetic stirrer running at 1250 rpm. Lyophilized/rehydrated cell-free products (or lyophilized TSB medium as OM control) were added to achieve a concentration of 100 mg/ml. The films do not contain lyophilized M18 supernatant products or OM were also used as controls ("blank" film). To ensure complete swelling and hydration, the mixture was left to stand for 1 h after mixing and then stirred at 1250 rpm at 40 °C following the addition of the plasticizer. Subsequently, the solution was allowed to settle undisturbed for 15 min. at 37 °C to eliminate air bubbles. The prepared mixtures were poured onto surfaces such as parafilm, glass, polystyrene, wax paper, cling film, and stainless steel using the solvent casting method, but it was observed that the films were most easily detached from the silicone surface. Additionally, since silicone can withstand high temperatures, it is autoclavable, which is an important feature for ensuring sterile conditions in biological activity experiments. Thus, the solutions prepared as described above were poured into 1 cm^3 volume (1 cm x 1 cm, cubic) silicone molds, as 750 µl, left at RT for overnight (16 h) to prevent rapid drying and deformation, and then dried at 37 °C for 24 h (Ouda et al. 2020). The different film formulations were evaluated for flexibility, transparency, ease of assembly, easy pourability, easy peeling from the surface, drying parameters and appropriate combinations (polymer and plasticizer type) and the suitable amounts of the film components (appropriate amount and ratios of polymer and plasticizer) were determined through optimization studies (Ouda et al. 2020).

The films were removed from the silicon molds and cut into 1 cm^2 pieces using scissors. The formulations were then exposed to UV-C (254 nm) for 30 min. to 3 h in a sterile cabinet for sterilization before being used in biological activity analyses. The efficiency of UV-C treatment was analyzed by dissolving the blank film (1 cm^2) in 250 µl of TSB medium and incubating the medium in a shaking incubator (160 rpm) at 37 °C for 24 h. At the end of incubation, the turbidity of the medium was measured at 600 nm. The optimal film formulation for loading with cell-free products of the probiotic was determined based on both the physical characterization and sterility of the films achieved through UV-C exposure.

The films were characterized also for weight and thickness. Randomly selected film samples (1 cm^2; 8 pieces) were weighted using an analytical balance and thickness measurements at three random points on three randomly selected films were made using a digital thickness gauge (±0.01 mm; Piranha, Turkey). To be used in disintegration/dissolution and biological activity analyses (anti-pathogen and anti-cancer activities; please see below), the films were stored at + 4ºC in a desiccator in the dark.

Fourier-Transform Infrared Spectroscopy (FTIR) was employed to spectrally characterize the films, with a specific focus on identifying functional groups originating from bacterial products (Mohd Yusof et al. 2020) integrated into the ODF matrix. The FTIR absorption spectra of the films were recorded in the range of 400–4000 cm^{-1} by KBr disc method using FTIR spectrophotometer (Bala and Sharma 2018). For 3 randomly selected films (1 cm^2 each), 1/4 of the films were analyzed for blank (Blank-ODF; films without lyophilized medium or bacterial products), OM (OM-ODF), and M18 (M18-ODF) loaded ODFs. Spectra obtained from measurements were processed with baseline correction, peak normalization, and smoothing. Peaks were obtained using Spectragryph v1.2.16.1 trial version with a threshold of 5%, the significance level of 3, and the position tolerance of 0.4.

Disintegration and dissolution analyses along with loading and release assessments of the oral films

Release analyses were conducted in simulated salivary fluid (Roger et al. 2011) prepared as previously described by dissolving disodium hydrogen phosphate (0.2382%, w/v), potassium dihydrogen phosphate (0.019%, w/v), and sodium chloride (0.8%, w/v) in dH_2O (Koland et al. 2011). After adjusting the pH to 6.75 using phosphoric acid, the

simulated salivary fluid was sterilized through a 0.22 µm PES filter.

The methods outlined by Wasilewska and Winnicka were followed during disintegration and release analyses (Wasilewska and Winnicka 2019). For sample collection during disintegration determination and release analyses, 7 ml simulated salivary fluid was heated to 37ºC in a 10 cm petri dish. 1 cm^2 films were immersed in the pre-heated saliva solution and thoroughly mixed by stirring at 200 rpm using a 4 cm magnetic stir bar on a 37ºC magnetic stirrer. Samples (100 µl) were collected at 2, 5, 10, and 20 min. for FTIR analyses. FTIR spectra were collected in transmission mode using the KBr pellet (Ruiz-Rubio et al. 2018). Briefly, a 10 µl sample was impregnated on a KBr plate, and the spectra were obtained with a Brucker Vertex 70 V in the range of 400–4000 cm^{-1}. Data were collected using Opus 5.5 software. Spectra were recorded at RT with 1 cm^{-1} spectral resolution, with a total of 32 scans collected. Vector normalized spectra were used for principal component analysis (PCA) to differentiate release profiles of the ODFs.

Disintegration times and complete dissolution times of the films were also recorded during release experiments. Of note, after complete dissolution, the pH of the saliva medium was also measured using a pH meter to evaluate if the pH of the environment changed by the ODF.

Analysis of the anti-growth activity of probiotics's cell-free supernatant on *Streptococcus mutans*

For anti-pathogen activity analysis, *S. mutans* (ATCC 35668) was grown overnight at 37 °C with shaking at 160 rpm in TSB medium as previously mentioned (Vaziriamjad et al. 2022; Doğan and Tunçer Çağlayan 2024). 10^3 colony-forming units-CFU/ml were incubated with the cell-free supernatant or its lyophilized/rehydrated form (Karaçam and Tunçer 2023). After 24 h incubation at 37 °C with shaking, the viability of the pathogen was determined by monitoring OD_{600} values. After incubation, the pathogen viability was also assessed by agar spotting assay. For this, cultures were serially diluted in TSB and 3 µl of both diluted and undiluted (UD = undiluted) bacteria were dropped onto TSA plates (Karaçam and Tunçer 2022). The agar plates were incubated overnight at 37 °C and then visualized using the Gel Logic-212 Pro imaging system (Carestream, USA). The experiments were repeated as two biological replicates each with two technical replicates.

The anti-pathogenic activity of ODFs containing lyophilized M18 cell-free supernatant against *S. mutans* was investigated in an artificial saliva environment which was prepared as described above. Initially, a 1 cm^2 film was completely dissolved in 1 ml simulated salivary fluid. The dissolved film (resulting from the complete dissolution of a 1 cm^2 film in 1 ml saliva) or its dilutions at 1:2 and 1:4 ratios in the simulated salivary fluid were inoculated with *S. mutans* (10^3 CFU/ml), previously incubated overnight in TSB. Bacterial growth was determined by measuring the OD_{600} of cultures incubated at 37 °C with shaking at 160 rpm for 24 h. Besides turbidity measurements, agar spot assays were conducted after 24 h of incubation as described above. The experiments were carried out with two randomly chosen ODFs.

Analysis of the orally dissolving films for anti-proliferative activity on colon cancer cells *in vitro*

The human colorectal cancer cell line HCT-116 (DSMZ, Germany) was cultured in RPMI-1640 medium (pH 7.4) containing 10% fetal bovine serum (FBS), 1% penicillin-streptomycin (pen/strep; 100 U/ml), and 2 mM L-glutamine at 37 °C in a 5% CO_2 incubator. For subculturing, cells were washed with PBS (Phosphate-Buffered Saline) and detached with 0.25% trypsin-EDTA.

MTT (3-(4,5-dimethylthiazol-2-yl)-2,5-diphenyltetrazolium bromide) assay is used to measure cellular metabolic activity as an indicator of cell viability, proliferation, and cytotoxicity. The growth inhibitory effect of the ODF on HCT-116 cells was analyzed by using an MTT reagent (BioVision, Pennsylvania, USA) as described before (Tunçer et al. 2019; Karaçam and Tunçer 2022). Briefly, the day before, cells were seeded in 96-well plates at a density of 10^4 cells/well (100 µl). On the day of the experiment, a 1 cm^2 film (film containing lyophilized OM or lyophilized cell-free supernatant of M18) was completely dissolved in a 1 ml culture medium. To assess whether the ODFs affect the pH of the cancer cell culture medium, pH was determined using pH strips. Ensuring the film did not affect the buffering capacity of the medium, HCT-116 cells incubated with the dissolved film in the culture medium and its dilutions (1:2 and 1:4 dilution ratios) for 4, 14, and 24 h. After removing the culture media at the end of the incubation period, 100 µl RPMI-1640 culture medium containing 1.2 µM MTT was added to the wells, and the plates were incubated at 37 °C for 4 hours. After incubation, 100 µl SDS-HCl solution (0,01 M HCl containing 1 g/10 ml SDS) was added to the wells for the dissolution of MTT formazans, and the plates were incubated at 37 °C for 16 h. Absorbance was measured at 570 nm using a microplate reader (Thermo Fisher Scientific). The values obtained from the wells without cell seeding were used as blanks. Morphological changes in cells were observed under a light microscope (Nikon Eclipse TS100, Japan) and photographed with an HD camera (Toupcam, China) (Karaçam and Tunçer 2022). Two randomly chosen ODFs were used in the experiments.

Statistical analysis

All studies were conducted with at least two biological replicates each with at least two technical replicates. Graphs and the statistical significance of the data obtained from analyses were determined using Prism 8.01 (GraphPad, CA, USA). Results are presented as mean ± SEM, and differences at the level of $p \leq 0.05$ were considered statistically significant (*$p \leq 0.05$; **$p \leq 0.01$; ***$p \leq 0.001$; ****$p \leq 0.0001$).

Results

The cell-free supernatant of *Streptococcus salivarius* M18 exhibits anti-growth effect on *Streptococcus mutans*

M18 has been shown to inhibit the growth of specific strains of *S. mutans in vitro* and reduce *S. mutans* counts in clinical studies (Gong et al. 2023; Reichardt et al. 2024). Therefore, before incorporating it into ODF forms, the cell-free supernatant of the probiotic was evaluated on *S. mutans* both before and after lyophilization to assess whether the cell-free supernatant also exhibits anti-pathogen activity. As depicted in Fig. 1a, the cell-free supernatant inhibited growth by approximately 70% compared to the OM. The inhibition decreased when the supernatant from the probiotic was diluted within the growth medium (at ratios of 1:2 and 1:4). This suggests that the cell-free supernatant from M18 reduces pathogen growth concentration dependently. After reconstitution in dH_2O, the lyophilized probiotic supernatant was incubated with *S. mutans*. Figure 1b demonstrates the inhibitory effect of the lyophilized supernatant on pathogen growth, also indicating a concentration-dependent response.

Please note that *S. mutans* is acidogenic, contributing to caries through the production of acidic metabolites that corrode the tooth surface and demineralize calcium, ultimately leading to cavity formation (Tian et al. 2024). *S. mutans* becomes more pathogenic in an acidic environment, thriving when the pH is around 5.0 or lower. Although *S. mutans* is present in the mouths of healthy individuals, it generally remains non-competitive under the mouth's normal pH conditions. However, environmental changes, such as increased intake of fermentable sugars, can make the plaque environment more acidic, favoring *S. mutans* growth and promoting caries. This low-pH environment enhances *S. mutans* competitiveness under acidic conditions (Friedman 2011). The ecological plaque hypothesis suggests that disease can be prevented by addressing the environmental factors that enable pathogenic bacteria to overpopulate; for *S. mutans*, this means reducing acidic conditions (Marsh 2004; Friedman 2011). In summary, to simulate the pH conditions of a healthy oral cavity (nearly neutral saliva pH), the pH of the probiotic's supernatant (as well as its lyophilized and rehydrated form) was adjusted to 7.0, also taking into account that salivary buffering capacity decreases when the pH falls below 5.5. (Zhang et al. 2022).

Orally dissolving film formulations were optimized for loading with lyophilized cell-free supernatant

Before preparing lyophilized probiotic supernatant in the form of ODF, different ODF formulations were prepared to evaluate their film-forming properties. For this purpose, the film-forming success of different formulations was investigated using 0.6% w/v HPMC or 0.6% w/v HPMC + 0.6%, 1.0%, and 1.5% w/v GG with 0.1% w/v sorbitol. Mixtures formed with increasing concentrations of GG were found to be highly viscous and contained air bubbles, making them unsuitable for homogeneous film casting. The film prepared with 0.6% w/v HPMC + 0.6% w/v GG + 0.1% w/v sorbitol, on the other hand, formed a preferred formulation in terms of casting and mold release (Supplemental Fig. 1a). However, UV sterilization experiments conducted on the film using UV-C (254 nm) revealed that the film was not suitable for UV sterilization: even after UV-C sterilization extended up to 3 h, bacterial growth detected by OD_{600} in the culture medium where the film was incubated. Although UV-C sterilization has been reported for HPMC (Dave et al. 2013), it absorbs light in the UV-C region (254 nm) significantly in water (Suma and Sangappa 2022). In this study, sorbitol was chosen as the plasticizer for its potential prebiotic activity, while it does not contribute to the formation of dental caries (Pérez-Ramos et al. 2017). However, similar to HPMC, sorbitol also has significant absorbance for UV-C (Srivastava et al. 2022). Therefore, the absorption profiles of HPMC and sorbitol may have reduced the effectiveness of UV-C sterilization. Thus, glycerol was used in further optimization studies instead of sorbitol as the plasticizing agent (Rani 2017).

For the designed ODF formulation, UV sterilization was chosen due to concerns regarding the potential degradation of bacterial products (as well as film components) at high temperatures, which may occur during moist heat or dry heat sterilization. Therefore, film optimization experiments were conducted using alternative film-forming agents suitable for UV-C sterilization. Various film formulations were prepared, incorporating Carboxymethyl Cellulose (CMC), GG, and sodium alginate (SA) as film-forming agents, along with glycerol as plasticizers. CMC, a cellulose derivative, is widely accepted in the pharmaceutical industry due to its hydrophilicity, biocompatibility, and low immunogenicity across a range of traditional and advanced

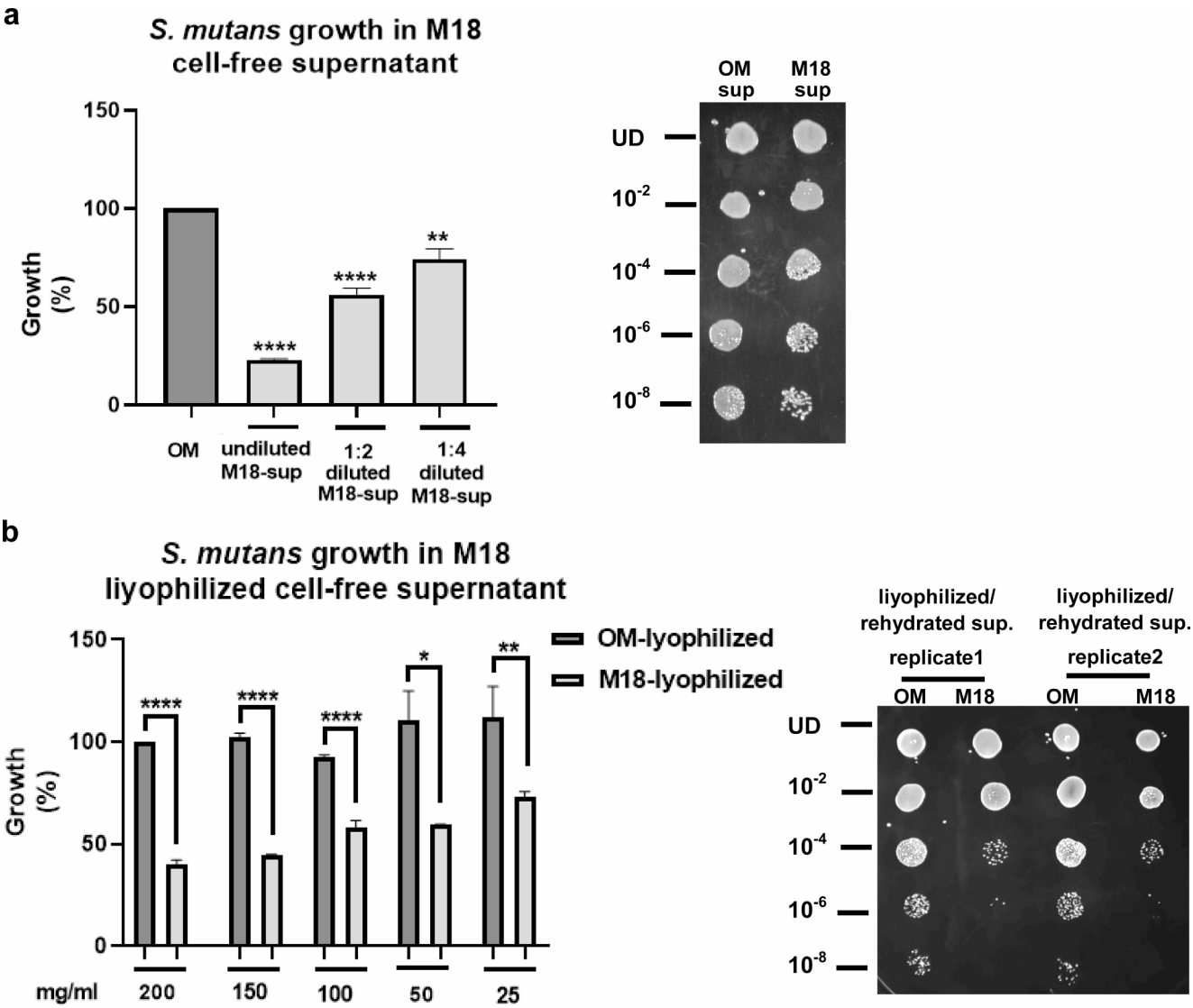

Fig. 1 Anti-growth activity of *S. salivarius* M18 on *S. mutans*: **a**. The antibacterial activity of the *S. salivarius* M18 cell-free supernatant, either undiluted or diluted in growth medium at ratios of 1:2 or 1:4, is presented as a percentage relative to the OM control and was statistically analyzed in comparison to the OM control. Growth inhibition (with undiluted supernatant) was also evaluated by agar spot plating (on the right). **b**. The effect of the lyophilized/rehydrated strain M18 cell-free supernatant was evaluated on *S. mutans* by measuring optical densities at 600 nm, and the results were presented relative to the liyophilized/rehydrated OM control (200 mg/ml). Agar spot plating results, from two biological replicates carried out with the 100 mg/ml lyophilized products, are shown on the right

dosage forms. However, the ionization of carboxylic groups in CMC's chemical structure renders it highly susceptible to water absorption, resulting in films with weak mechanical integrity and rapid drug release (Alruwaili et al. 2022). As such, composite film formulations were explored using CMC (at concentrations of 0.1% w/v or 0.6% w/v) and GG (at concentrations of 0.1% w/v or 0.6% w/v); however, these formulations did not yield satisfactory results in terms of mechanical properties: the resulting films were fragile, prone to fragmentation, or challenging to de-mold from silicone molds. Therefore, optimization studies continued with food-grade CMC-E466 as a supporting agent and food-grade SA-E401 as a film-forming agent. SA was preferred not only for its film-forming properties (Rani 2017; Khalid and Selmin 2022) but also for its prebiotic activity (Wang et al. 2006). Films were evaluated for demolding, fragility, and flexibility properties by observation, and the combination of 1.0% w/v CMC + 1.0% w/v SA + 0.5% w/v glycerol was found to be successful in terms of form (Supplemental Fig. 1b).

After successfully creating the film, the possibility of sterilization with UV was investigated. It was previously reported that CMC (Mansouri et al. 2020) and alginate (Derkach et al. 2020) do not absorb at 254 nm. Films were

left in UV for 30 min, 1 h or 2 h and then incubated in TSB medium as described above for 24 h at 37 °C with agitation at 160 rpm. Depending on OD_{600} absorbance measurements, 30 min. UV treatment was found suitable for sterilization: mean OD_{600} was 0.049 for the three independent ODF incubated medium and 0.053 for the blank medium. However, it was observed that adding lyophilized products (100 mg/ml OM or M18 cell-free supernatant lyophilized products) reduced the flexibility of the films. Consequently, the amount of glycerol, the plasticizing agent, was increased from 0.5% w/v to 1.0% w/v glycerol. Supplemental Fig. 1c displays the films created with the combination of 1.0% w/v CMC + 1.0% w/v SA + 1.0% w/v glycerol formulation. Since the TSB medium has a yellowish-brown color [8], OM and M18 films can be distinguished from the blank film.

The thickness and the weights of the films are presented in Table 1. The ODFs were described to have thicknesses ranging from 12 to 100 µm (Wasilewska and Winnicka 2019). Accordingly, the produced prototypes adhere to the standard thicknesses of ODFs. When considering the weights per 1 cm^2 surface area, the blank film (Blank-ODF; without lyophilized product) has an approximate density of 0.198 g/cm^3, the film containing lyophilized culture medium (OM-ODF) has a mean density of 0.844 g/cm^3, and the film containing lyophilized probiotic supernatant (M18-ODF) has a mean density of 0.824 g/cm^3. The lower density of the Blank-ODF may be due to voids in the film structure, while the increased density in OM and M18 films compared to the blank film indicates successful loading.

As a note, following the dissolution of the films in simulated saliva (as discussed in the next section), the pH of the saliva was measured for three separate film samples, resulting in a pH of 6.55 ± 0.7 for OM-ODF and 6.63 ± 0.15 for M18-ODF. The pH of the simulated saliva was measured under the same conditions and found to be 6.65 ± 0.07. Therefore, it can be concluded that the postbiotic-containing film prototype had no significant impact on the pH of the saliva.

The prepared oral films were characterized for FTIR. The mean spectra belonging to Blank-ODF, OM-ODF, and M18-ODF are presented in Supplemental Fig. 2 and the major absorption peaks obtained from these spectra are given in Table 2 with their corresponding assigned vibrations.

Since all three films contain CMC and SA, characteristic peaks corresponding to these components are shared by all three films. Various -OH vibration modes related to the polymeric skeleton (peaks between 3647.9-3447.3 cm^{-1} and 3229.7-1942.9 cm^{-1}) are observed in all three films. Additionally, C = O vibrations observed around 1772, 1749, 1734, and 1717 cm^{-1} probably represent groups belonging to CMC and/or SA. Characteristic peaks observed around 1684, 1636, and 1577 cm^{-1} corresponding to -COO stretching, C = O stretching, and -COOH, respectively, also confirm the polymeric structure. Various C-H vibrations listed in the same table are also observed in all three films (around 1559, 1540, 1521.5, 1507, 1489.9, around 1472.7, and 1457.3 cm^{-1}). Along with various C-H vibrations, -OH and O-C-O vibrations also indicate common structures shared by the films. The characteristic peaks common to both OM-ODF and M18-ODF, arising from components of the growth medium, include around 1792 cm^{-1} for C = O symmetric stretching, and around 1762 cm^{-1} for C = O vibration, and the relevant Amid I bands around 1653 and 1623 cm^{-1}. Additionally, characteristic peaks observed in both OM and M18 films include around 1085 cm^{-1} for PO_2 symmetric, around 1436.5 cm^{-1} for C-H deformation, and around 1700 cm^{-1} for C = O vibration associated with fatty acid esters. The characteristic peaks obtained exclusively in M18 films, on the other hand, are assigned for the probiotic-related biological activity. Exclusively in M18-ODF, in the Amid I region, peaks at 3309.6 cm^{-1} for the Amid A band, the characteristic 1669.1 cm^{-1} peak for anti-parallel β-sheet (Amid I), and 1646.8 cm^{-1} for Amid I random coil, 310 or α-helices were observed. The characteristic peak observed at 1569.8 cm^{-1} in the Amid II region confirms the presence of proteins originating from the M18 cell-free supernatant as for the characteristic peak observed at 1318.9 cm^{-1}, a component of the Amid III band of proteins. Additionally, peaks were observed at 1923.1 cm^{-1} for CH_2 asymmetric stretching, 1448.2 cm^{-1} for the CH_2 bending associated with lipids/CH_2 deformation of protein and lipids and anti-symmetric bending vibration of CH_3 group, 1405.1 cm^{-1} for CH3 asymmetric deformation of triglycerides and N-H bending in amine group, 1114 cm^{-1} for symmetric stretching of P-O-C, 1362.8 cm^{-1} for symmetric bending of lipid CH_3, and 1339.7 cm^{-1} for phenyl ring stretching accompanied by planar C-O stretching vibration in M18-ODF samples. The peaks obtained only in M18 films indicating the presence of oligonucleotides are as follows: 1374.7 cm^{-1} for cytosine, guanine C-N stretching, 989.3 cm^{-1} for RNA stretching and uracil ring bending, 852.7 cm^{-1} for left-handed helical DNA (Z-form), 830.8 cm^{-1} for sugar C2' endo conformation, 792.8 cm^{-1} for guanine in the C3' endo/syn conformation of DNA's Z conformation, and 781.7 cm^{-1} for guanine. In summary, the unique peaks detected solely in the M18-ODF samples serve as evidence of the successful integration of bacterial biomolecules into the ODF matrix.

Table 1 The thickness and weights of the ODFs

Characterization (per ODF with 1 cm^2 surface area)	Blank-ODF	OM-ODF	M18-ODF
Thickness (µm)	30,00 ± 7,07	32,67 ± 5,65	39,33 ± 15,20
Weight (mg)	5,96 ± 3,19	26,91 ± 4,86	32,38 ± 9,63

Table 2 IR absorption bands and assignments for the ODFs

Wavenumber (cm^{-1})			Assignment	Reference
Blank-ODF	OM-ODF	M18-ODF		
3647.9	3648.8	3649.2	Various -OH vibrational peaks	(Choo et al. 1995; Li et al. 2004; Mossoba et al. 2005; Lee et al. 2015; Talari et al. 2017)
3628.6	3628.8	3629.1		
3587.2	3587	3587.5		
3566.7	3566.6	3567		
3545.5	3545.7	3545.7		
3537	3536.8	3536.6		
3523.6	3523.4	3523.9		
3480.7	3481.4	3481.5		
3447.3	3447.6	3447.6		
		3309.6	Amid A band	(Wang et al. 2011)
3229.7	3233.5	3229	-OH symmetric stretching	(Talari et al. 2017)
2065.3	2065.2	2065.3	-OH stretching	(Li et al. 2004)
1992.6	1992.5	1992.4	The band of second order	(Talari et al. 2017)
1967.6	1967.5	1967.5		
1942.9	1942.9	1942.9		
		1923.1	CH_2 asymmetric stretching	(Shulga et al. 2011)
		1868.9	†Free -OH	(Hody et al. 2006)
	1792.2	1792.3	C = O symmetric stretching	(Sclavons et al. 2005)
1772.2	1772.2	1772.3	C = O stretching, attributed to alginate	(Othman et al. 2020)
	1761.7	1761.9	C = O vibration, protein, Asp	(Fahmy et al. 1993)
1748.7	1749.1	1749.3	‡-COOH	(El-Nahas et al. 2021)
1734	1734	1734.1	Asymmetric stretching vibration of -COOH groups attributed to alginate	(Kenawy et al. 2019)
1717.5	1717.3	1717.5	‡C = O stretching	(Uyanga et al. 2020)
	1699.8	1700	C = O vibration, fatty acid ester	(Dovbeshko et al. 2000)
1684	1684	1684.1	-COO asymmetric stretching	(Wen et al. 2014)
		1669.1	Amid I (anti-parallel β-sheet)	(Wong et al. 1991)
	1653	1653.2	Amid I	(Noreen et al. 2011)
		1646.8	Random coil, 310 or α-helices of Amid I	(Dave et al. 2000; Cobb et al. 2020)
1636.1	1636.2	1636	C = O stretching of carbonyl group	(Talari et al. 2017)
	1623.4	1623.7	Amid I	(Schubert et al. 2010)
1576.7	1576.6	1576.6	‡Stretching absorption of -COOH	(Rozali et al. 2015)
		1569.8	Amid II	(Taylor et al. 2011)
1559.1	1559	1559.1	C-H aromatic stretching	(Dogan et al. 2016)
1540	1540.1	1540.1	C = O stretching attributed to CMC	(Li et al. 2020)
1521.5	1521.5	1521.6	‡C = C stretching of aromatic ring	(Ndruru et al. 2019)
1507.1	1507.2	1507.3	‡C-H bending	(Li et al. 2004)
1489.9	1489.9	1489.9		
1472.7	1472.8	1472.9		
1457.3	1457.3	1457.4	‡CH_3 asymmetric bending	(Junhom et al. 2016)
		1448.2	CH_2 bending associated with lipids/CH_2 deformation of protein and lipids Antisymmetric bending vibration of CH_3 group	(Lyman and Fay 2014; Mehta et al. 2020) (Dong and Ozaki 1997; Mani et al. 2023)
	1436.5	1436.6	C-H bending	(Tingaut et al. 2011)
1419	1418.8	1418.8	‡C = O symmetric stretching	(Ebrahiminezhad et al. 2019)
		1405.1	CH_3 asymmetric deformation of triglycerides N-H bending in amine group	(Crocco et al. 2023) (Maria and Simonescu 2012)
1395	1395.2	1395.6	-OH bending, -CH_2- twisting and wagging (attributed to CMC)	(Karimi et al. 2016)
1384.7	1384.8	1385.3	C-H stretching, C-O vibration and C-OH stretching (attributed to CMC)	(Gasemloo et al. 2016; Invernizzi et al. 2018)
		1374.7	Stretching C-N cytosine, guanine	(Talari et al. 2017)

Table 2 (continued)

Wavenumber (cm^{-1})			Assignment	Reference
Blank-ODF	OM-ODF	M18-ODF		
		1362.8	CH_3 symmetric bending of lipids	(Mostaço-Guidolin et al. 2010)
		1339.7	In-plane C-O stretching vibration combined with the ring stretch of phenyl	(Talari et al. 2017)
		1318.9	Amide III band components of proteins	(Singh 2000; Talari et al. 2017)
		1114	Symmetric stretching P-O-C	(Movasaghi et al. 2008)
	1085	1085.5	PO_2 symmetric; phospholipids, and partially protein (amide III). The band originating from sugar chains (C-OH band) overlaps	(Talari et al. 2017)
1056.4	1056.5	1056.8	C-O stretching (attributed to glycerol)	(Abo El-Reesh et al. 2020)
1047.5	1045.8	1046.9	‡C-OH and C-O stretching vibration found in polysaccharides	(Menzies et al. 2014; Castillo et al. 2019; Yang et al. 2021; Hammes et al. 2024)
		989.3	RNA stretching, ring bending of uracil	(Talari et al. 2017)
		852.7	Left-handed DNA helix (Z-form)	(Mossoba et al. 2005)
		830.8	C2' endo conformation of sugar	(Talari et al. 2017)
		792.8	Guanine in a C3'endo/syn conformation in the Z conformation of DNA	(Talari et al. 2017)
		781.7	Guanin	(Cayrol et al. 2009)
720.6	720.3	720.5	‡C-H stretching	(Ramírez-Hernández et al. 2019)
649.1	648.5	648.9	C-H asymmetric	(Cai et al. 2016)
634.8	634.8	635.4	OH out-of-plane bend (associated)	(Shetty et al. 2006; Talari et al. 2017)
526.2	526.0	525.7	‡deformation of C-C-O and C-CH_3	(Güven et al. 2019)
516.5	517.7	517.5	‡O-C-O bonds	(Yoğurtcuoğlu 2023)

†NaOH was used to adjust the pH of the probiotic cell-free supernatant as described in the Materials and Methods section

‡Probably from CMC and/or SA

Spectral characterizations of the films suggest the dissolution of biomolecules, originating from probiotic cell-free supernatant, into the simulated saliva

ODFs can be divided into three categories based on dissolution potential. Films that dissolve within 1–30 s. are termed fast-dissolving ODFs; films that dissolve within 1–30 min. are known as moderately dissolving ODFs; and slow-dissolving ODFs can take more than 30 min. to dissolve (Gupta et al. 2020). Here, disintegration analysis revealed that the films initiate disintegration within 2 min., and complete disintegration is achieved in 9–10 min. Figure 2 illustrates the differences in content released into the simulated saliva over time, represented by PCA applied to ATR-FTIR spectral data at these analyzed time points. Release analyses of Blank-ODF, OM-ODF, and M18-ODF were conducted at 2 min. (Fig. 2a), 5 min. (Fig. 2b), and 10 min. (Fig. 2c), with additional analysis at 20 min. (Fig. 2d), where complete dissolution was observed. The loading plots showing differences in the PC1 and PC2 planes compared to the reference spectra for Blank-ODF are presented in Supplemental Fig. 3. The data in Fig. 2 indicate that at every time point, the release profiles differ among the ODF groups, and a substantial proportion of the variance (PC1) can be explained by the growth medium content: no medium for Blank-ODF and lyophilized medium for OM-ODF and M18-ODF. Additionally, the second principal component (PC2) seems to correspond to the bioactive ingredients of the probiotic's cell-free supernatant present in the M18-ODF, which can be distinguished from the OM-ODF. Finally, Fig. 3 presents the time-dependent PCA analysis of the FTIR data from saliva release experiments for Blank-ODF (Fig. 3a), OM-ODF (Fig. 3b), and M18-ODF (Fig. 3c). Overall, the PCA results indicate significant differences in the time-dependent release into saliva across all films. However, it is noteworthy that M18-ODFs demonstrate the most substantial separation (95.8%; 90.2% for PC1 and 5.6% for PC2) among all data points, indicating the highest degree of distinction in time-dependent release compared to OM and Blank-ODFs.

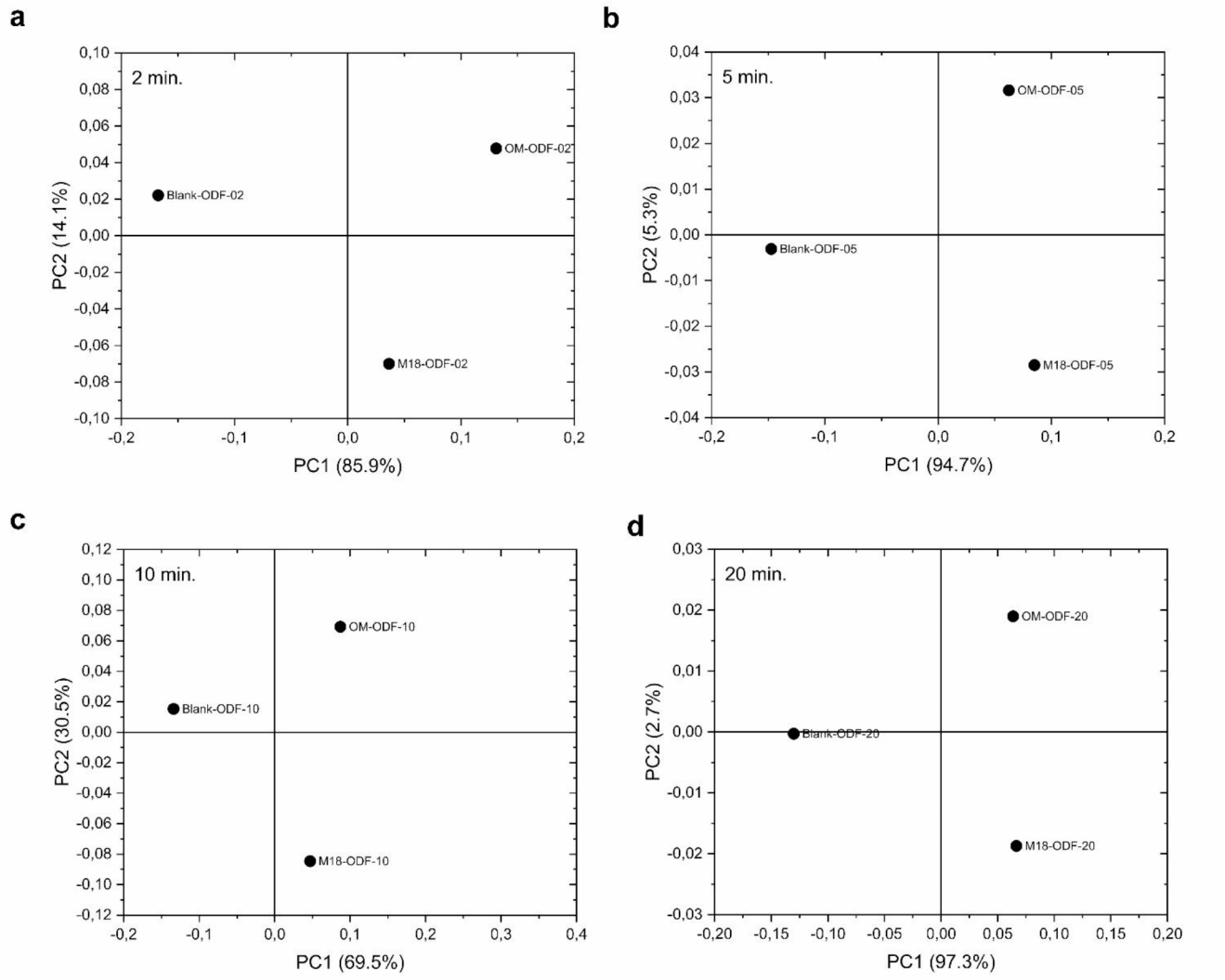

Fig. 2 PCA analysis results of ODF (Blank, OM and M18-ODFs) content in simulated saliva conducted after (**a**) 2, (**b**) 5, (**c**) 10, and (**d**) 20 min

Orally dissolving film prepared with lyophilized *Streptococcus salivarius* M18 cell-free supernatant shows anti-growth activity on *Streptococcus mutans* and anti-proliferative activity on cancer cells *in vitro*

For the anti-pathogenic activity tests, the growth of *S. mutans* was analyzed after treating the pathogen with the dissolved film (resulting from the complete dissolution of a 1 cm^2 film in 1 ml saliva) or its dilutions at 1:2 and 1:4 ratios in saliva for 24 h. The results of the turbidity measurements and agar spot assays show that the M18-ODF has growth inhibitory activity on *S. mutans* (Fig. 4a).

Bioactive molecules in the cell-free supernatant of probiotic bacteria have gained attention in recent years for their anti-cancer activities (Chauhan et al. 2021; Karaçam and Tunçer 2022). Previous study has shown that M18 cell-free supernatant inhibits the growth of colon cancer cells and induces cell death (Karaçam and Tunçer 2022). Thus, in this study, the anti-cancer effect of the M18 cell-free supernatant in ODF form was evaluated on the HCT-116 human colon cancer cell line. Figure 4b shows that the ODF prepared with the cell-free supernatant of *S. salivarius* M18 inhibited cancer cell proliferation, with inhibition increasing alongside ODF concentration. Notably, the pH of the growth medium remained stable after dissolving the M18-ODFs (Supplemental Fig. 4), as also observed in the simulated saliva. Since the oral and buccal mucosa are highly vascularized, agents loaded into ODFs are expected to penetrate and enter systemic circulation without passing through the digestive system. Pre-gastric absorption from the mouth, pharynx, and esophagus is reported to enhance therapeutic effects as the agent disintegrates in the mouth (Chandramouli et al. 2023). Although probiotic-derived anti-cancer molecules require sophisticated design for

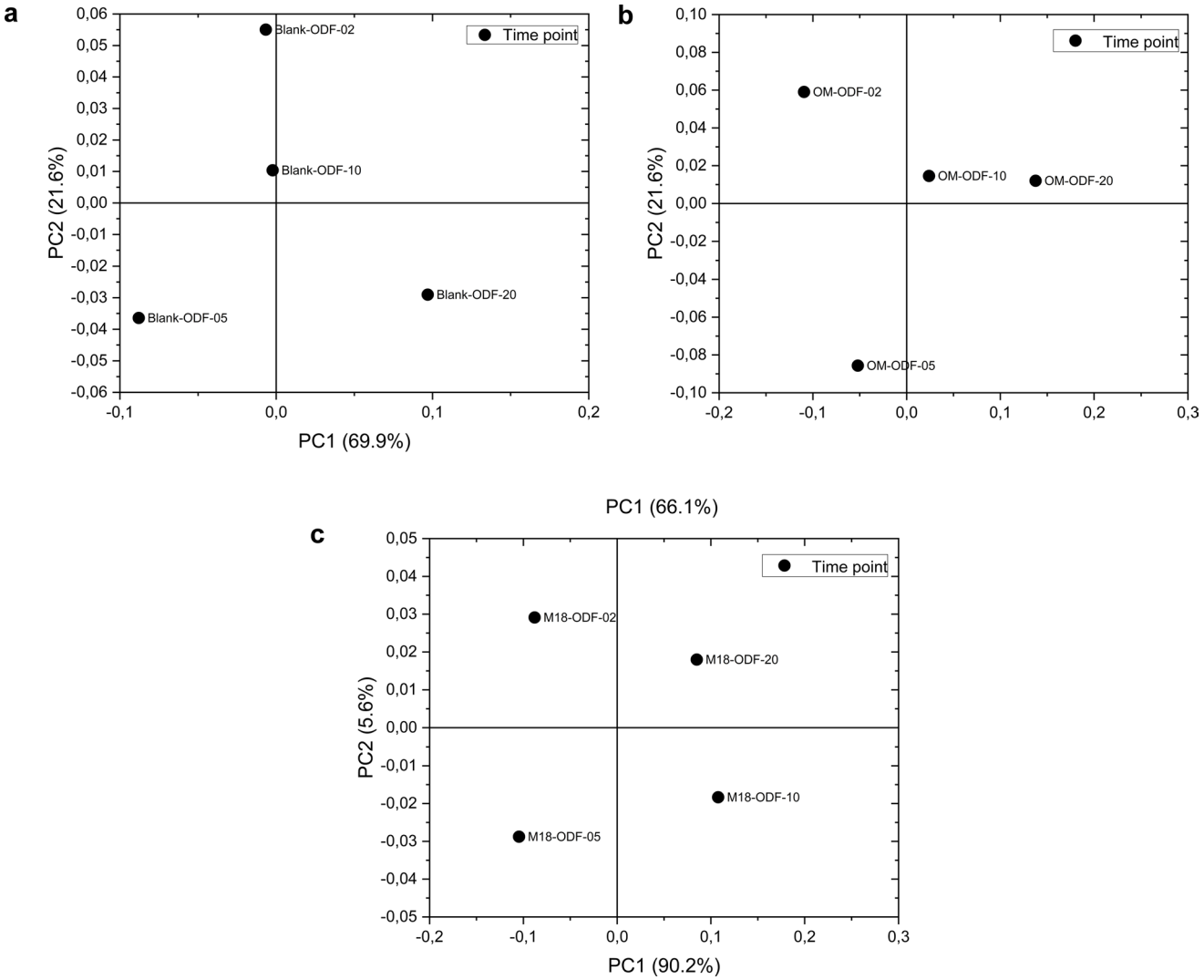

Fig. 3 Time-dependent differentiation of ODF contents in simulated saliva assessed by PCA analyses for (**a**) Blank-ODF, (**b**) OM-ODF, and (**c**) M18-ODF over 2, 5, 10, and 20 min

targeted therapies (e.g., gastro-retentive or colon-active delivery systems) (Deshayes et al. 2021), ODFs can serve as a dosage platform for anti-cancer agents designed to reach their target either by passing through the digestive system, via pre-gastric absorption, or through systemic circulation. From this perspective, the anti-cancer molecules present in the probiotic supernatant warrant further investigation.

Discussion

Numerous studies have confirmed the close relationship between oral microbiota composition and oral health, highlighting its disruption as a crucial step in oral diseases. *S. mutans*, a key bacterium in oral microflora, is recognized as a primary cause of dental decay and a biofilm-forming agent. While various factors contribute to tooth decay, microbial factors are considered predominant, suggesting bacteriotherapy as a promising approach for oral disease prevention (Homayouni Rad et al. 2023). In recent years, probiotics and their derived postbiotics, as cell-free supernatants, have gained significant recognition for their health-promoting effects (El Far et al. 2023).

In this manuscript, the cell-free supernatant of the well-recognized oral probiotic *S. salivarius* M18 was incorporated into a biopolymer film. Following several optimization studies, the ODFs intended for probiotic loading were formulated using carboxymethyl cellulose (CMC) and sodium alginate (SA), with glycerol serving as a plasticizer. CMC, a derivative of cellulose (the most abundant biopolymer), is favored in the pharmaceutical industry for its swelling capacity, biodegradability, stability, non-cytotoxicity, biocompatibility, non-immunogenicity, and cost-effectiveness (Morozkina et al. 2022). SA, known for its significant

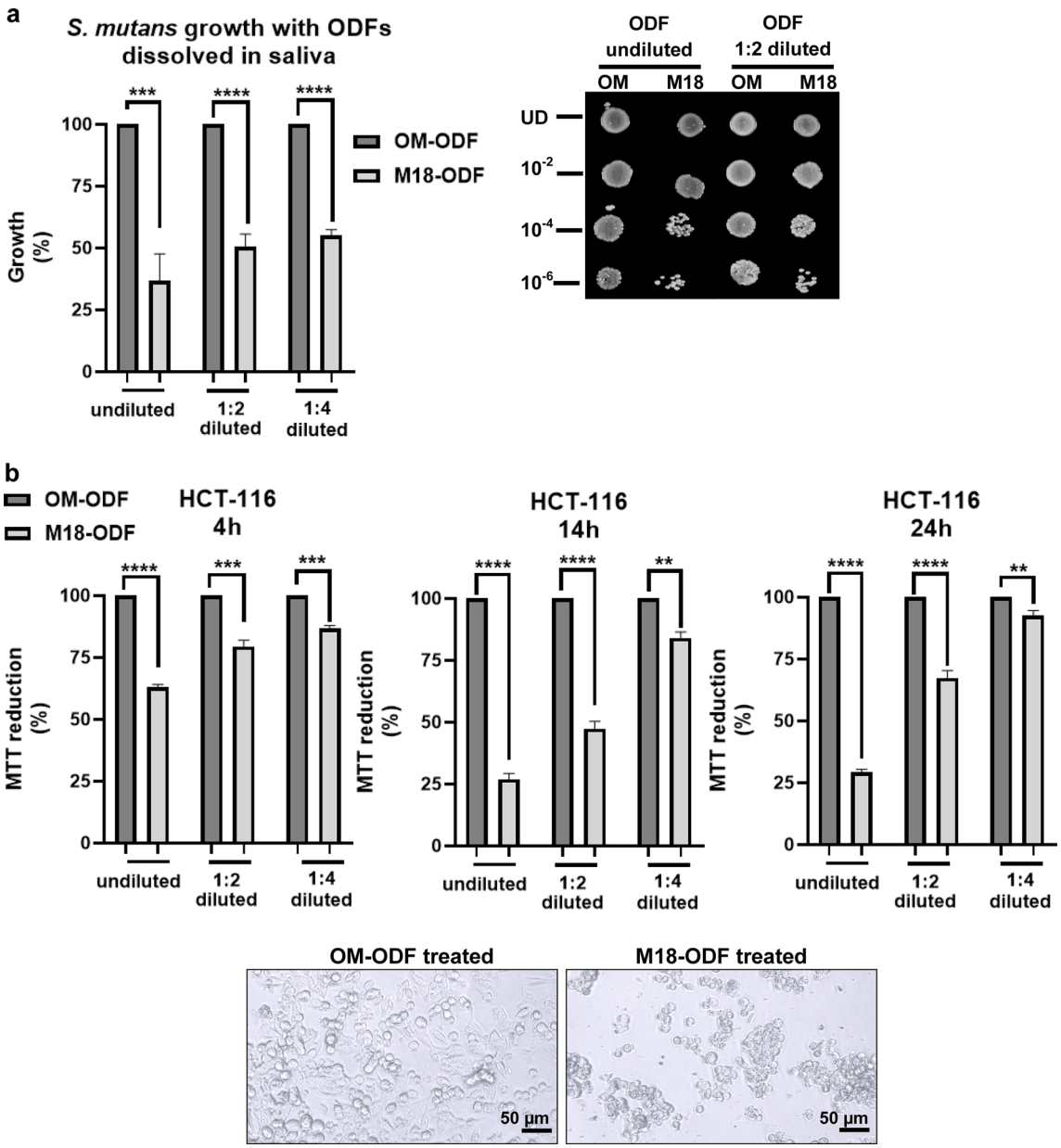

Fig. 4 Growth inhibitory activity of the ODF incorporated with lyophilized probiotic supernatant was investigated against (**a**) the oral pathogen *S. mutans* and (**b**) the colon cancer cell line HCT-116. The ODFs were used either directly after dissolution or in 1:2 and 1:4 dilutions. Results are presented as percentages relative to corresponding OM-ODF controls. For the anti-pathogen activity analysis, the ODFs were completely dissolved in simulated saliva, incubated with *S. mutans* for 24 h, and growth inhibition was assessed by OD_{600} measurements (left) and further confirmed by spot plating (right). For anti-cancer activity analysis, the films were dissolved in culture media, and cell growth was determined through MTT assay at 4, 14, and 24 h post-treatment. The lower panel shows light microscope images of HCT-116 cells treated with undiluted OM-ODF or M18-ODF after 14 h of treatment

rheological effects such as gelation, thickening, and dispersion stabilization, as well as its biocompatibility, biodegradability, non-genotoxicity, and biostability, was utilized to not only enhance the rheological properties of the CMC films but also to support their adhesive properties (Morozkina et al. 2022). Furthermore, alginate has been reported to possess health-promoting prebiotic activities (Wang et al. 2006), making it a valuable addition to thin film formulations alongside its film-forming effects. The incorporation of glycerol had a positive impact on the mechanical characteristics of the films by mitigating brittleness (Paolicelli et al. 2018), particularly in samples loaded with bacterial products which tended to reduce film flexibility. As detailed in the results section, in addition to rheological properties, the sterilization capability (to be suitable for sterilization) of the ODFs is also addressed as a drawback. Interestingly, much

of the literature does not discuss or assess the sterility of oral films. Here, it is demonstrated that the composition of CMC, SA, and glycerol resulted in the production of flexible and non-brittle films that can be sterilized using UV-C. Finally, the ODF incorporated with probiotic products demonstrated bioactive effects against the oral pathogen *S. mutans* (without compromising probiotic activity) and also showed activity against epithelial cancer cells.

Conclusions

This manuscript demonstrates that probiotics's metabolites, as emerging concepts in functional biotics, can be integrated into bio-based ODFs and show promise as multifaceted ingredients for commercialization.

Data Availability

All the data generated during and/or analyzed during the current study are available from the corresponding author on reasonable request.

Supplementary Information The online version contains supplementary material available at https://doi.org/10.1007/s00203-024-04207-w.

Acknowledgements The author acknowledges the Molecular Biology and Genetics Department and the Biotechnology Application and Research Center of Bilecik Şeyh Edebali University for providing laboratory facilities, Dr. Zafer Üstündağ and the Physics Department of Dumlupınar University for access to the ATR-FTIR facility, Dr. Fadime Özdemir (Bilecik Şeyh Edebali University) for technical support regarding the lyophilizer, and Sevinç Karaçam (Bilecik Şeyh Edebali University) for technical assistance during the optimization experiments for the polymer-ODF. The author gratefully thanks Dr. Mustafa Oğuzhan Çağlayan (Bilecik Şeyh Edebali University) for engaging in discussions on FTIR data analyses.

Author contributions S.T.Ç. designed the study, carried out the experiments, analyzed the results, and wrote the manuscript.

Funding This work is supported by Bilecik Şeyh Edebali University, Scientific Research Fund (2022-01.BŞEÜ.12 – 01) to STÇ.

Data availability No datasets were generated or analysed during the current study.

Declarations

Ethical approval This project does not contain any studies with human or animal subjects.

Informed consent For this type of study, consent is not required.

Competing interests The authors declare no competing interests.

Conflict of interest The author declares no competing financial interests or personal relationships that could have appeared to influence the work reported in this paper.

References

Abikshyeet P, Mishra P, Bhuyan L et al (2022) Probiotics: dawn of a new era in dental caries management. J Pharm Bioallied Sci. https://doi.org/10.4103/jpbs.jpbs_801_21

Abo El-Reesh GY, Farghali AA, Taha M, Mahmoud RK (2020) Novel synthesis of Ni/Fe layered double hydroxides using urea and glycerol and their enhanced adsorption behavior for cr(VI) removal. Sci Rep 10:587. https://doi.org/10.1038/s41598-020-57519-4

Alruwaili NK, Ahmad N, Alzarea AI et al (2022) Arabinoxylan-Carboxymethylcellulose Composite films for antibiotic delivery to infected wounds. Polym (Basel) 14:1–16. https://doi.org/10.3390/polym14091769

Bala R, Sharma S (2018) Formulation optimization and evaluation of fast dissolving film of aprepitant by using design of experiment. Bull Fac Pharm Cairo Univ. https://doi.org/10.1016/j.bfopcu.2018.04.002

Baliga S, Muglikar S, Kale R (2013) Salivary pH: a diagnostic biomarker. J Indian Soc Periodontol. https://doi.org/10.4103/0972-124X.118317

Cai L, Chen T, Wang W et al (2016) Optimization of aluminum/silicon compounds on fire resistance of old corrugated container fiber foam material. BioResources. https://doi.org/10.15376/biores.11.3.6505-6517

Castillo LA, López OV, García MA et al (2019) Crystalline morphology of thermoplastic starch/talc nanocomposites induced by thermal processing. Heliyon. https://doi.org/10.1016/j.heliyon.2019.e01877

Cayrol B, Geinguenaud F, Lacoste J et al (2009) Auto-assembly of E. Coli DsrA small noncoding RNA: molecular characteristics and functional consequences. RNA Biol. https://doi.org/10.4161/rna.6.4.8949

Chandramouli M, Shivalingappa RP, Basavanna V et al (2023) Oral thin-films from design to delivery: a Pharmaceutical viewpoint. Biointerface Res Appl Chem. https://doi.org/10.33263/BRIAC132.177

Chauhan S, Dhawan DK, Saini A, Preet S (2021) Antimicrobial peptides against colorectal cancer-a focused review. Pharmacol Res 167:105529. https://doi.org/10.1016/j.phrs.2021.105529

Choo L-P, Mansfield JR, Pizzi N et al (1995) Infrared spectra of human central nervous system tissue: diagnosis of alzheimer's disease by multivariate analyses. Biospectroscopy. https://doi.org/10.1002/bspy.350010208

Chugh P, Dutt R, Sharma A et al (2020) A critical appraisal of the effects of probiotics on oral health. J Funct Foods

Cobb JS, Zai-Rose V, Correia JJ, Janorkar AV (2020) FT-IR Spectroscopic Analysis of the secondary structures Present during the Desiccation Induced Aggregation of Elastin-Like polypeptide on silica. ACS Omega. https://doi.org/10.1021/acsomega.0c00271

Crocco MC, Moyano MFH, Annesi F et al (2023) ATR-FTIR spectroscopy of plasma supported by multivariate analysis discriminates multiple sclerosis disease. Sci Rep 13:2565. https://doi.org/10.1038/s41598-023-29617-6

Dave N, Troullier A, Mus-Veteau I et al (2000) Secondary structure components and properties of the Melibiose Permease from Escherichia coli: a Fourier Transform Infrared Spectroscopy Analysis. Biophys J 79:747–755. https://doi.org/10.1016/S0006-3495(00)76332-6

Dave V, Paliwal S, Yadav S (2013) Formulation and evaluation of controlled delivery of aceclofenac through ocular insert. Turkish J Pharm Sci 10(2):205–220.

Derkach SR, Voron'ko NG, Sokolan NI et al (2020) Interactions between gelatin and sodium alginate: UV and FTIR studies. J Dispers Sci Technol. https://doi.org/10.1080/01932691.2019.1611437

Dogan NM, Sensoy T, Doganli GA et al (2016) Immobilization of lycinibacillus fusiformis B26 cells in different matrices for use in turquoise blue HFG decolourization. Arch Environ Prot. https://doi.org/10.1515/aep-2016-0013

Doğan K, Tunçer Çağlayan S (2024) Capsaicin shows species and strain-specific activity: investigation of the Antibacterial effects on the oral Pathogen Streptococcus mutans and the oral probiotics Streptococcus salivarius M18 and K12. Hacettepe J Biol Chem 52:11–19. https://doi.org/10.15671/hjbc.1337284

Dong J, Ozaki Y (1997) FTIR and FT-raman studies of partially miscible poly(methyl methacrylate)/poly(4-vinylphenol) blends in solid states. Macromolecules. https://doi.org/10.1021/ma9607168

Dovbeshko GI, Gridina NY, Kruglova EB, Pashchuk OP (2000) FTIR spectroscopy studies of nucleic acid damage. In: Talanta

Ebrahiminezhad A, Moeeni F, Taghizadeh SM et al (2019) Xanthan gum capped ZnO microstars as a promising dietary zinc supplementation. Foods. https://doi.org/10.3390/foods8030088

El Far MS, Zakaria AS, Kassem MA et al (2023) Promising biotherapeutic prospects of different probiotics and their derived postbiotic metabolites: in-vitro and histopathological investigation. BMC Microbiol 23:122. https://doi.org/10.1186/s12866-023-02866-1

El-Nahas S, Arafat AS, El Din HS et al (2021) A Novel Alternative methods for Decalcification of Water resources using Green agro-ashes. Molecules 26:6777. https://doi.org/10.3390/molecules26226777

Fahmy K, Weidlich O, Engelhard M et al (1993) Aspartic acid-212 of bacteriorhodopsin is ionized in the M and N photocycle intermediates: an FTIR study on specifically 13 C-labeled reconstituted purple membranes. Biochemistry. https://doi.org/10.1021/bi00073a020

Friedman JY (2011) The role of Streptococcus Mutans in the formation of Dental Caries: an ecological perspective. Sci J Lander Coll Arts Sci 5:40–46

Gasemloo S, Sohrabi MR, Khosravi M et al (2016) Fabrication of sulfated nanofilter membrane based on carboxymethyl cellulose. Water Sci Technol 74:2611–2619. https://doi.org/10.2166/wst.2016.441

Gong S-G, El-shennawy S, Choudhary P et al (2023) Antimicrobial activity of probiotic Streptococcus salivarius LAB813 on in vitro cariogenic biofilms. Arch Oral Biol 154:105760. https://doi.org/10.1016/j.archoralbio.2023.105760

Gupta MS, Kumar TP, Gowda DV (2020) Orodispersible thin film: a new patient-centered innovation. J Drug Deliv Sci Technol

Güven B, Duraklı-Velioğlu S, Boyacı İH (2019) Rapid Identification of some sweeteners and sugars by attenuated total reflectance-fourier transform Infrared (Atr-Ftir), Near-Infrared (Nir) and Raman Spectroscopy. Gıda 44:274–290. https://doi.org/10.15237/gida.gd18119

Hammes N, Pinheiro C, Segundo IR et al (2024) Coaxial fibres incorporated with phase change materials for thermoregulation applications. Appl Sci 14:2473. https://doi.org/10.3390/app14062473

He M, Zhu L, Yang N et al (2021) Recent advances of oral film as platform for drug delivery. Int J Pharm 604:120759. https://doi.org/10.1016/j.ijpharm.2021.120759

Heng C (2016) Tooth decay is the most prevalent disease. Fed Pract 33:31–33

Hody V, Belmonte T, Pintassilgo CD et al (2006) Modification of hexatriacontane by O2-N2 microwave post-discharges. Plasma Chem Plasma Process. https://doi.org/10.1007/s11090-006-9017-3

Homayouni Rad A, Pourjafar H, Mirzakhani E (2023) A comprehensive review of the application of probiotics and postbiotics in oral health. Front Cell Infect Microbiol 13. https://doi.org/10.3389/fcimb.2023.1120995

Invernizzi C, Rovetta T, Licchelli M, Malagodi M (2018) Mid and near-infrared reflection spectral database of natural organic materials in the cultural heritage field. Int J Anal Chem 2018:1–16. https://doi.org/10.1155/2018/7823248

Javed K, Nasir MZ, Jalees M, Manzoor MA (2023) Role of diet and dietary habits in causing dental caries among adults reporting to a tertiary care hospital in Pakistan; a case-control study. Heliyon 9:e23117. https://doi.org/10.1016/j.heliyon.2023.e23117

Jung J-I, Baek S-M, Nguyen TH et al (2021) Effects of Probiotic Culture Supernatant on Cariogenic Biofilm formation and RANKL-Induced osteoclastogenesis in RAW 264.7 macrophages. Molecules 26:733. https://doi.org/10.3390/molecules26030733

Junhom C, Weerapreeyakul N, Tanthanuch W, Thumanu K (2016) FTIR microspectroscopy defines early drug resistant human hepatocellular carcinoma (HepG2) cells. Exp Cell Res. https://doi.org/10.1016/j.yexcr.2015.12.007

Karaçam S, Tunçer S (2022) Exploiting the acidic extracellular pH: evaluation of Streptococcus salivarius M18 postbiotics to target cancer cells. Probiotics Antimicrob Proteins 14:995–1011. https://doi.org/10.1007/s12602-021-09806-3

Karaçam S, Tunçer S (2023) Lyophilized cell-free supernatants of the oral probiotics Streptococcus salivarius M18 and Streptococcus salivarius K12 show promises for milk safety. Lett Appl Microbiol 76:1–10. https://doi.org/10.1093/lambio/ovac034

Karimi S, Feizy J, Mehrjo F, Farrokhnia M (2016) Detection and quantification of food colorant adulteration in saffron sample using chemometric analysis of FT-IR spectra. RSC Adv. https://doi.org/10.1039/c5ra25983e

Kenawy ER, Azaam MM, El-nshar EM (2019) Sodium alginate-g-poly(acrylic acid-co-2-hydroxyethyl methacrylate)/montmorillonite superabsorbent composite: Preparation, swelling investigation and its application as a slow-release fertilizer. Arab J Chem. https://doi.org/10.1016/j.arabjc.2017.10.013

Khalid M, Selmin G F (2022) Applications of alginates in the design and preparation of orodispersible dosage forms. In: Properties and applications of alginates. IntechOpen

Koland M, Vijayanarayana K, Charyulu Rn, Prabhu P (2011) In vitro and in vivo evaluation of Chitosan buccal films of ondansetron hydrochloride. Int J Pharm Investig 1:164. https://doi.org/10.4103/2230-973x.85967

Koliarakis I, Messaritakis I, Nikolouzakis TK et al (2019) Oral bacteria and intestinal dysbiosis in colorectal cancer. Int J Mol Sci 20:4146. https://doi.org/10.3390/ijms20174146

Kudra A, Muszyński D, Sobocki BK et al (2023) Insights into oral microbiome and colorectal cancer – on the way of searching new perspectives. Front Cell Infect Microbiol 13. https://doi.org/10.3389/fcimb.2023.1159822

Lee JH, Kim HG, Lee WJ (2015) Characterization and tissue incorporation of cross-linked human acellular dermal matrix. Biomaterials. https://doi.org/10.1016/j.biomaterials.2014.12.004

Li X, Lin J, Ding J et al (2004) Raman spectroscopy and fluorescence for the detection of liver cancer and abnormal liver tissue. In: Annual International Conference of the IEEE Engineering in Medicine and Biology - Proceedings

Li Z, Kuang H, Yang J et al (2020) Improving emulsion stability based on ovalbumin-carboxymethyl cellulose complexes with thermal treatment near ovalbumin isoelectric point. Sci Rep. https://doi.org/10.1038/s41598-020-60455-y

Lyman DJ, Fay SG (2014) The effect of breast cancer on the Fourier transform infrared attenuated total reflection spectra of human hair. Ecancermedicalscience. https://doi.org/10.3332/ecancer.2014.405

Mani N, Suresh S, Govindammal M et al (2023) Spectroscopic (FT-IR, FT-Raman, NMR and UV–visible), ADMET and molecular

docking investigation of aztreonam as anti-tuberculosis agent. Chem Phys Impact. https://doi.org/10.1016/j.chphi.2023.100254
Mansouri L, Benghanem S, Elkolli M, Mahmoud B (2020) Chemical and biological behaviours of hydrogels based on oxidized carboxymethylcellulose coupled to Chitosan. Polym Bull. https://doi.org/10.1007/s00289-019-02712-3
Maria C, Simonescu CM (2012) Application of FTIR spectroscopy in environmental studies. In: Advanced aspects of spectroscopy. InTech
Marsh PD (2004) Dental plaque as a microbial biofilm. Caries Res 38:204–211. https://doi.org/10.1159/000077756
Mehta M, Naffa R, Maidment C, et al (2020) ATR-FTIR spectroscopy towards classification, of wet blue bovine leather using ratiometric and chemometric analysis. J Leather Sci Eng. https://doi.org/10.1186/s42825-019-0017-5
Menzies GE, Fox HR, Marnane C et al (2014) Fourier transform infrared for noninvasive optical diagnosis of oral, oropharyngeal, and laryngeal cancer. Transl Res. https://doi.org/10.1016/j.trsl.2013.09.006
Mohd Yusof H, Abdul Rahman N, Mohamad R et al (2020) Biosynthesis of zinc oxide nanoparticles by cell-biomass and supernatant of Lactobacillus plantarum TA4 and its antibacterial and biocompatibility properties. Sci Rep 10:19996. https://doi.org/10.1038/s41598-020-76402-w
Morozkina S, Strekalovskaya U, Vanina A et al (2022) The fabrication of Alginate–Carboxymethyl Cellulose-based composites and Drug Release profiles. Polym (Basel) 14:3604. https://doi.org/10.3390/polym14173604
Morrison AG, Sarkar S, Umar S et al (2023) The contribution of the human oral microbiome to oral disease: a review. Microorganisms 11:318. https://doi.org/10.3390/microorganisms11020318
Mossoba MM, Al-Khaldi SF, Kirkwood J et al (2005) Printing microarrays of bacteria for identification by infrared microspectroscopy. In: Vibrational Spectroscopy
Mostaço-Guidolin LB, Murakami LS, Batistuti MR et al (2010) Molecular and chemical characterization by Fourier transform infrared spectroscopy of human breast cancer cells with estrogen receptor expressed and not expressed. Spectroscopy. https://doi.org/10.3233/SPE-2010-0466
Movasaghi Z, Rehman S, ur Rehman DI (2008) Fourier transform infrared (FTIR) spectroscopy of biological tissues. Appl Spectrosc Rev 43:134–179
Ndruru STCL, Wahyuningrum D, Bundjali B, Arcana IM (2019) Green simple microwave-assisted extraction (MAE) of cellulose from Theobroma cacao L. (TCL) husk. In: IOP Conference Series: Materials Science and Engineering
Noreen R, Chien CC, Delugin M et al (2011) Detection of collagens in brain tumors based on FTIR imaging and chemometrics. Anal Bioanal Chem. https://doi.org/10.1007/s00216-011-4899-1
Othman NZ, Hanapi NSM, Saim N et al (2020) Selective determination of acidic drugs in water samples using online solid phase extraction liquid chromatography with alginate incorporated multi-walled carbon nanotubes as extraction sorbent. Indones J Chem. https://doi.org/10.22146/ijc.43703
Ouda GI, Dahmash EZ, Alyami H, Iyire A (2020) A novel technique to Improve Drug Loading Capacity of Fast/Extended release orally dissolving films with potential for paediatric and geriatric drug delivery. AAPS PharmSciTech. https://doi.org/10.1208/s12249-020-01665-5
Paolicelli P, Petralito S, Varani G et al (2018) Effect of glycerol on the physical and mechanical properties of thin gellan gum films for oral drug delivery. Int J Pharm 547:226–234. https://doi.org/10.1016/j.ijpharm.2018.05.046
Pérez-Ramos A, Werning ML, Prieto A et al (2017) Characterization of the sorbitol utilization cluster of the probiotic Pediococcus parvulus 2.6: genetic, functional and complementation studies in heterologous hosts. Front Microbiol. https://doi.org/10.3389/fmicb.2017.02393
Ramírez-Hernández A, Aguilar-Flores C, Aparicio-Saguilán A (2019) Fingerprint analysis of ftir spectra of polymers containing vinyl acetate. DYNA. https://doi.org/10.15446/dyna.v86n209.77513
Rani TN (2017) Formulation Development and optimization of oral thin films of Zolpidem Tartarate. Med Sci Healthc Pract. https://doi.org/10.22158/mshp.v1n1p26
Reichardt E, Shyp V, Alig L et al (2024) Antimicrobial effect of probiotic bacteriocins on Streptococcus mutans biofilm in a dynamic oral flow chamber model–an in vitro study. J Oral Microbiol. https://doi.org/10.1080/20002297.2024.2304971
Roger P, Delettre J, Bouix M, Béal C (2011) Characterization of Streptococcus salivarius growth and maintenance in artificial saliva. J Appl Microbiol. https://doi.org/10.1111/j.1365-2672.2011.05077.x
Rozali MLH, Ahmad Z, Isa MIN (2015) Interaction between carboxy methylcellulose and salicylic acid solid biopolymer electrolytes. Adv Mater Res 1107:223–229 https://doi.org/10.4028/www.scientific.net/amr.1107.223
Ruiz-Rubio L, Alonso ML, Pérez-álvarez L et al (2018) Formulation of Carbopol®/poly(2-ethyl-2-oxazoline)s mucoadhesive tablets for buccal delivery of hydrocortisone. Polym (Basel). https://doi.org/10.3390/polym10020175
Schubert JM, Bird B, Papamarkakis K et al (2010) Spectral cytopathology of cervical samples: detecting cellular abnormalities in cytologically normal cells. Lab Investig. https://doi.org/10.1038/labinvest.2010.72
Sclavons M, Laurent M, Devaux J, Carlier V (2005) Maleic anhydride-grafted polypropylene: FTIR study of a model polymer grafted by ene-reaction. Polym (Guildf). https://doi.org/10.1016/j.polymer.2005.06.115
Shetty G, Kendall C, Shepherd N et al (2006) Raman spectroscopy: elucidation of biochemical changes in carcinogenesis of oesophagus. Br J Cancer. https://doi.org/10.1038/sj.bjc.6603102
Shulga E, Pohako K, Treshchalov A et al (2011) Functionalisation of aligned carbon nanotubes with nitric acid vapour. Micro Nano Lett. https://doi.org/10.1049/mnl.2011.0357
Singh BR (2000) Basic aspects of the technique and applications of infrared spectroscopy of peptides and proteins. ACS Symp Ser. https://doi.org/10.1021/bk-2000-0750.ch001
Spatafora G, Li Y, He X et al (2024) The evolving microbiome of dental caries. Microorganisms
Srivastava B, Sen S, Sen K (2022) Free serum sorbitol and its interaction with caffeine: a suggestive approach for plausible remediation of diabetic neuropathy. Biotechnol Appl Biochem. https://doi.org/10.1002/bab.2083
Suma SB, Sangappa Y (2022) Fabrication and characterization of HPMC-AuNPs nanocomposite films. Mater Today Proc 54:660–663. https://doi.org/10.1016/j.matpr.2021.10.361
Talari ACS, Martinez MAG, Movasaghi Z et al (2017) Advances in fourier transform infrared (FTIR) spectroscopy of biological tissues. Appl Spectrosc Rev 52:456–506. https://doi.org/10.1080/05704928.2016.1230863
Taylor SE, Cheung KT, Patel II et al (2011) Infrared spectroscopy with multivariate analysis to interrogate endometrial tissue: a novel and objective diagnostic approach. Br J Cancer. https://doi.org/10.1038/sj.bjc.6606094
Tian S, Ding T, Li H (2024) Oral microbiome in human health and diseases. mLife 3:367–383. https://doi.org/10.1002/mlf2.12136
Tingaut P, Hauert R, Zimmermann T (2011) Highly efficient and straightforward functionalization of cellulose films with thiol-ene click chemistry. J Mater Chem. https://doi.org/10.1039/c1jm11620g
Tunçer S, Karaçam S (2020) Cell-free supernatant of Streptococcus salivarius M18 impairs the pathogenic properties of Pseudomonas

aeruginosa and Klebsiella pneumonia. Arch Microbiol. https://doi.org/10.1007/s00203-020-02005-8

Tunçer S, Çolakoğlu M, Ulusan S et al (2019) Evaluation of colloidal platinum on cytotoxicity, oxidative stress and barrier permeability across the gut epithelium. Heliyon 5. https://doi.org/10.1016/j.heliyon.2019.e01336

Uyanga KA, Okpozo OP, Onyekwere OS, Daoud WA (2020) Citric acid crosslinked natural bi-polymer-based composite hydrogels: Effect of Polymer ratio and beta-cyclodextrin on hydrogel microstructure. React Funct Polym. https://doi.org/10.1016/j.reactfunctpolym.2020.104682

Vaziriamjad S, Solgi M, Kamarehei F et al (2022) Evaluation of L-arginine supplement on the growth rate, biofilm formation, and antibiotic susceptibility in Streptococcus mutans. Eur J Med Res 27:108. https://doi.org/10.1186/s40001-022-00735-7

Wang Y, Han F, Hu B et al (2006) In vivo prebiotic properties of alginate oligosaccharides prepared through enzymatic hydrolysis of alginate. Nutr Res. https://doi.org/10.1016/j.nutres.2006.09.015

Wang X, Qi Z, Wang S et al (2011) The study of a single BGC823 cell using Fourier transform infrared microspectroscopic imaging. Spectrochim Acta - Part Mol Biomol Spectrosc. https://doi.org/10.1016/j.saa.2011.05.031

Wasilewska K, Winnicka K (2019) How to assess orodispersible film quality? A review of applied methods and their modifications. Acta Pharm 69:155–176. https://doi.org/10.2478/acph-2019-0018

Wen P, Gong P, Mi Y et al (2014) Scalable fabrication of high quality graphene by exfoliation of edge sulfonated graphite for supercapacitor application. RSC Adv. https://doi.org/10.1039/c4ra04788e

Wong PTT, Papavassiliou ED, Rigas B (1991) Phosphodiester stretching bands in the Infrared Spectra of Human tissues and cultured cells. Appl Spectrosc. https://doi.org/10.1366/0003702914335580

Yang K, Luo X, Zhai Y et al (2021) Influence of sodium alginate on the gelatinization, rheological, and retrogradation properties of rice starch. Int J Biol Macromol 185:708–715. https://doi.org/10.1016/j.ijbiomac.2021.06.207

Yoğurtcuoğlu E (2023) Investigation of the effect of cyanidation after microwave roasting treatment on refractory gold/silver ores by characterization studies. Physicochem Probl Min Process. https://doi.org/10.37190/ppmp/157487

Zhang D, Jiang H, Chen J, Wang X (2022) Buffering capacity of saliva influences the perception of acid-related sensory properties. Food Qual Prefer. https://doi.org/10.1016/j.foodqual.2021.104454